Research article

Journal of RAMAN SPECTROSCOPY

Received: 24 May 2012 Revised: 25 June 2012 Accepted: 28 June 2012 Published online in Wiley Online Library: 5 September 2012

(wileyonlinelibrary.com) DOI 10.1002/jrs.4156

Thickness and stacking geometry effects on high frequency overtone and combination Raman modes of graphene

Dongfei Li,[a,b] Da Zhan,[a]* Jiaxu Yan,[a] Chenglin Sun,[b] Zuowei Li,[b] Zhenhua Ni,[c] Lei Liu[d] and Zexiang Shen[a]*

We investigate two high frequency Raman overtone and combination modes of graphene named 2D′ and 2D + G bands, and located at ~3240 and ~4260 cm^{-1}, respectively. The graphene thickness and stacking geometry effects for these two modes are systematically studied. The features of the 2D′ band, which arises from intravalley double resonance, are not sensitive to the variation of thickness with single Lorentzian peak and fixed linewidth. We explain it theoretically by calculating the phonon dispersion mode in *k*-space and find that the flat band region of longitudinal optical phonon near Γ point is the mechanism leading to the 2D′ band nonsplit. With the thickness increasing, the band position exhibits blueshift and the linewidth increases for the 2D + G band. With changing thickness and stacking geometry of graphene, the intensities of these two high-frequency bands show obvious different evolution compared with that of G band.

Supporting information can be found in the online version of this article.

Keywords: graphene; Raman; electronic band structure; double resonance; high frequency phonon modes

Introduction

Graphene, a two-dimensional (2D) allotrope of carbon where carbon atoms are arranged in a hexagonal lattice, has become one of the most exciting research topics in recent years because of its distinctive electronic properties.[1] It consists of sp^2 carbon hexagonal network, in which strong covalent bonds are formed between two adjacent carbon atoms. It is one atomic layer thick, which is stable in two dimensions even under suspended condition. Graphene has attracted great attention not only because it is the ideal material to study the fundamental properties of two-dimensional nanostructures,[2,3] but also for its potential applications in future electronic devices.[4,5] Various techniques can be used to prepare graphene, including micromechanical cleavage[2] or chemical exfoliation from bulk graphite,[6,7] thermal decomposition of single crystal SiC wafers,[8] growth from metal-carbon melts,[9–11] and chemical vapor deposition of hydrocarbons on metal films.[12,13]

Raman spectroscopy is a powerful scientific tool to characterize advanced materials because of its nondestructivity, convenience and high throughput. Particularly for graphene-based materials, Raman spectroscopy is proved to be one of the most effective methods to characterize various properties,[14–16] such as thickness,[17] doping,[18,19] intercalation,[20,21] defects,[22,23] oxidation level,[24] stacking geometry,[25,26] thermal properties,[27–29] strain[30,31] and edge dynamics.[32–34] Furthermore, a most recent research demonstrated that Raman spectroscopy can be used to investigate the isotope effects on the graphene lattice dynamics.[35] To date, most of the properties probed by Raman are based on the analysis of features evolution of three major Raman active bands, D, G and 2D, of which the Raman shifts under 532 nm excitation are ~1350, ~1580 and ~2700 cm^{-1}, respectively. Actually, besides these three bands, graphene has many relatively weak Raman active bands, which are also significant for both fundamental understanding and practical research guidance. For example, most recently, Rao *et al*. and Cong *et al*. respectively observed some new Raman active overtone bands at the wavenumber region from 1600–2200 cm^{-1},[36,37] and Tan *et al*. investigated the interlayer shear mode called 'C' band at low-wavenumber region down to 31 cm^{-1}.[38] However, the reported papers of Raman bands for high wavenumber region (>3000 cm^{-1}) are very limited despite the fact that graphene possesses high-order overtone and combination Raman active modes in this region.[36,39] In this paper, we perform detailed investigations of thickness and stacking geometry effects on these high-frequency overtone and combination Raman modes in graphene.

* *Correspondence to: Zexiang Shen, Division of Phyiscs and Applied Phyiscs, School of Physical and Mathematical Sciences, Nanyang Technological University, 21 Nanyang Link, Singapore 637371. E-mail: zexiang@ntu.edu.sg*

Da Zhan, Division of Phyiscs and Applied Phyiscs, School of Physical and Mathematical Sciences, Nanyang Technological University, 21 Nanyang Link, Singapore 637371. E-mail: physicsor@gmail.com

a *Division of Physics and Applied Physics, Nanyang Technological University, Singapore, 637371, Singapore*

b *State Key Laboratory of Superhard Materials, College of Physics, Jilin University, Changchun, 130021, P. R. China*

c *Department of Physics, Southeast University, Nanjing, 211189, P. R. China*

d *Key Laboratory of Excited State Processes, Changchun Institute of Optics, Fine Mechanics and Physics (CIOMP), Changchun 130033, China*

Experimental

Graphene samples were prepared by conventional micromechanical cleavage method from highly ordered pyrolytic graphite (HOPG) on silicon wafer covered by 300 nm SiO_2.[2] Because both bilayer graphene (BLG) and trilayer graphene (TLG) show exotic electronic properties and attract great interest the same as that of single-layer graphene (SLG), we intentionally selected SLG, BLG and TLG as our samples in this paper. The layer number of each graphene sample was confirmed by optical contrast spectroscopy.[40] We also used 'water flush' method to prepare intentionally a 1 + 1 folded graphene,[25] and it is incommensurate BLG of which the interlayer is electronic decoupled as can be revealed by Raman spectrum.[25] Raman spectral measurements were carried out with a Renishaw confocal Raman system under backscattering configuration, with excitation laser wavelength of 532 nm and 100× objective lens (numerical aperture, NA = 0.95). The selected visible laser for probing these multiphonon involved resonant Raman active bands discussed in this paper is because of the strong intensity, or else, the intensity of these bands would be too weak to be probed by other lasers, for example, the UV laser.[41] The laser power is controlled below 0.5 mW to avoid possible laser-induced heating. Raman images with a spatial resolution of ~600 nm are realized with a piezo stage (step size 100 nm). Density-functional calculations were performed by the Quantum ESPRESSO code,[42] using a plane wave basis and Troullier–Martins norm-conserving pseudopotentials.[43] An energy cutoff of 110 Ry was used. Methfessel–Paxton smearing with an energy width of 0.03 Ry was adopted for the self-consistent calculations.[44] The Brillouin zone was sampled using a $48 \times 48 \times 1$ grid for the electronic structure. A $6 \times 6 \times 1$ grid was used for the phonon calculation to obtain the dynamical matrices. The dynamical matrices are calculated based on density-functional perturbation theory within the linear response.[45]

Results and discussion

Raman spectra of graphene samples are shown in Figure 1, including SLG, AB-stacked BLG (aBLG), incommensurate bilayer graphene (IBLG), ABA-stacked (Bernal stacking) and ABC-stacked (Rhombohedral stacking) TLG (denoted as aTLG and cTLG, respectively). The aTLG and cTLG are identified by the 2D band features as described in Fig. S1.[46,47] The G and 2D band regions are shown in Fig. 1(a), while the 2D′ and 2D + G bands are shown in Figs 1(b) and (c), respectively. It is well known that the dependence of the 2D band with different thickness and stacking geometry reflects the evolution of the electronic band structure because the activation of the 2D band needs participation of two D phonons (TO phonon around the K point in the Brillouin zone) to fulfil the intervalley double resonance.[19,48] In Fig. 1(a), the 2D band of SLG possesses only one single Lorentzian peak, but aBLG, aTLG and cTLG show multiple-peak shape with very broad full width of half maximum (FWHM). This is because the SLG has only one single electronic band,[49,50] and hence the two TO-phonon involved double resonant Raman process has only one pathway to resonance between the valence and conduction band, that is, only the TO-phonon with fixed frequency can participate into this special double resonant process.[17] When the thickness of graphene increases from SLG to aBLG, the electronic coupling between graphene layers leads the split of both conduction and valence bands[49] and hence there are four pathways that can fulfil the two TO-phonon involved double resonant Raman process.[17] It also means that four TO phonons possessing different momentums in *k*-space can be observed by Raman spectroscopy. Because the frequency of TO phonon disperses not flatly with respect to momentum at around K-point, these four different TO-phonons also possess different frequencies, which leads the 2D band of aBLG presenting a broad peak with large FWHM because it consists of four subpeaks. Therefore, the widening effect

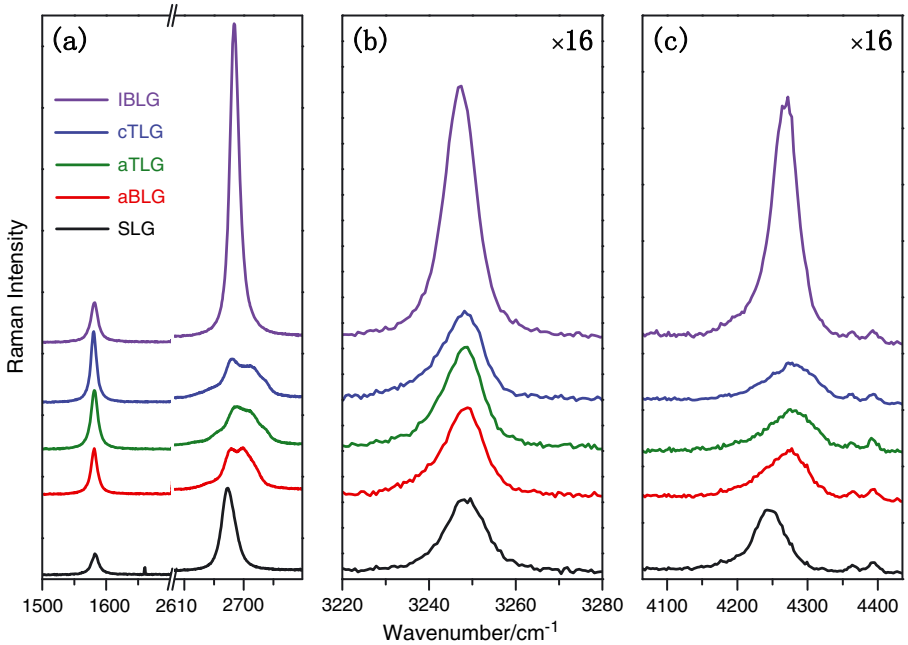

Figure 1. Raman spectra of SLG (black), aBLG (red), aTLG (green), cTLG (blue) and IBLG (purple). (a) The G and 2D bands region, (b) the 2D′ band region and (c) the 2D + G band region. This figure is available in colour online at wileyonlinelibrary.com/journal/jrs

of 2D band for the thicker graphene (layer number >2) with Bernal/Rhombohedral stacking geometry can also be explained.[17,46,47] It is worth noting that the two graphene layers of IBLG are electronically decoupled and its 2D band shows a very sharp single Lorentzian peak with slight stiffening effect compared with SLG.[25]

On the other hand, 2D′ band is another resonant Raman active mode in graphene and it is also directly correlated to graphene's electronic band structure, but the FWHM of the 2D′ band of graphene does not show any observable dependence on the thickness and stacking geometry (the Raman spectra of graphenes with various thickness and stacking geometry can be seen in Fig. 1(b)). The 2D′ band is activated by participation of two D′ phonons (longitudinal optical (LO) phonon near Γ point as is shown in Fig. 2(b)) to fulfil the intravalley double resonance.[16] Compared with SLG, the interlayer coupling induced energy band splitting at low-energy regime for Bernal/Rhombohedral stacking few-layer graphene are able to provide multiple pathways to satisfy the 2D′-phonon involved intravalley double resonant scattering. However, in our experiment, it is revealed that the FWHM of Bernal/Rhombohedral stacking few-layer graphene is the same as that of SLG, which is fixed at ~11 cm^{-1} as a constant. It means that the frequency difference among the D′ phonons scattered by different possible pathways can be neglected for few-layer graphene. This is obviously different from that of the aforementioned 2D band. An illustration of the double resonant process of 2D′ band of the aBLG case is shown in Fig. 2(a). There are four possible phonon scattering pathways that can fulfil the intravalley double resonant process (denoted by red, blue, green and purple dashed lines), and the corresponding phonon momentums are $\boldsymbol{q}_{22}$, $\boldsymbol{q}_{21}$, $\boldsymbol{q}_{12}$ and $\boldsymbol{q}_{11}$, respectively. The calculated phonon dispersion in *k*-space is shown in Fig. 2(b). There is a very restricted region near Γ point that the LO phonon disperses flatly with respect to *k*-space as indicated by arrows in Fig. 2(b). Thus, it is reasonable that the D′ phonons scattered from these four different Raman scattering pathways almost have the same frequency, which gives rise to the presentation of single Lorentzian peak because of the frequency degeneration. Furthermore, from another point of view, the wavevector of D′ phonon is very small as the D phonon arises from LO phonon dispersed at around Γ point (Fig. 2(b)),[16] and it means that the momentum differences among $\boldsymbol{q}_{22}$, $\boldsymbol{q}_{21}$, $\boldsymbol{q}_{12}$ and $\boldsymbol{q}_{11}$ are very small to satisfy the intravalley scattering. Thus, it is reasonable that the frequency difference among each D′ phonon scattered from different pathways is too small and can be ignored. The above mechanisms can also be used to explain the single 2D′ peak observed in *n*-layer graphene ($n > 2$) because the corresponding LO phonon dispersion curve in *k*-space is similar to that of aBLG.[51]

The combination mode of the 2D + G band is normally ignored by researchers, mainly because its intensity is very weak and the frequency region at ~4260 cm^{-1} is far away from the G and 2D band regions. The three-phonon involved Raman scattering process in $\vec{k}$-space is illustrated in Fig. 2(c). The process includes two D phonons with opposite momentum intervalley scattered, and followed by scattering another G phonon without momentum exchange. As shown in Fig. 1(b), the position of 2D + G band, pos (2D + G), blueshifts dramatically from SLG to aBLG, but it only

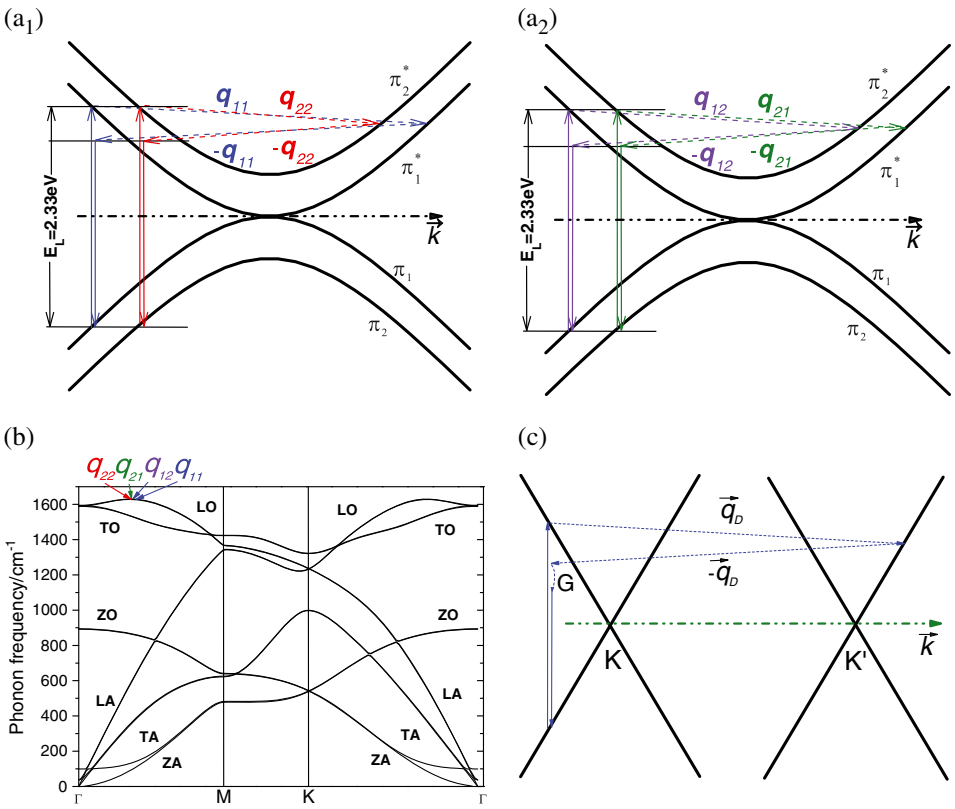

Figure 2. (a) Schematic intravalley double resonance process of 2D′ band in AB-stacked bilayer graphene. Four possible Raman scattering channels denoted by red, green, purple and blue dashed lines represent four LO phonons with different momentums. (b) The calculated phonon dispersion in $\vec{k}$-space of AB-stacked bilayer graphene. The red ($\boldsymbol{q}_{22}$), green ($\boldsymbol{q}_{21}$), purple ($\boldsymbol{q}_{12}$) and blue ($\boldsymbol{q}_{11}$) symbols represent four different phonon momentums arising from different Raman scattering channels, which indicates the energies of these four LO phonons degenerated in spite of their different momentums. (c) Schematic Raman scattering process for 2D + G band. This figure is available in colour online at wileyonlinelibrary.com/journal/jrs

slightly blueshifts when the number of layers further increases. Both the SLG and IBLG show a sharp 2D + G peak which can be fitted by single Lorentzian function, while aBLG, aTLG and cTLG show broader asymmetric peaks, which cannot be fitted by one Lorentzian function. Both the frequency and FWHM of 2D + G band have similar layer dependent behaviour as that of the 2D band, which indicates that such three-phonon involved Raman scattering process is also strongly dependent on the electronic band structure.[17]

It is well known that the thickness (number of layer) of few-layer graphene can be effectively estimated by the shape of the 2D band, and particularly the linewidth of the 2D band can let us accurately identify the number of layers.[17,22] The graphene's FWHM of 2D and 2D + G band varying with both the thickness and stacking geometry are shown in Fig. 3. It can be found that in addition to the 2D band, which shows FWHM dependence on both thickness and stacking geometry, the combination mode 2D + G also shows similar FWHM dependence trend on both the graphene thickness and stacking geometry to that of the 2D band. It is worth noting that both 2D and 2D + G bands present obvious broader peaks for cTLG compared with aTLG. Moreover, as can be seen in Fig. 4, for pos(2D + G)-based Raman mapping, it can let us easily identify SLG, aBLG, IBLG and aTLG. The graphene samples with different stacking geometry and thickness show obvious difference in terms of the band position, which mainly owes to the difference of their electronic band structures at low-energy region that close to the Dirac point.

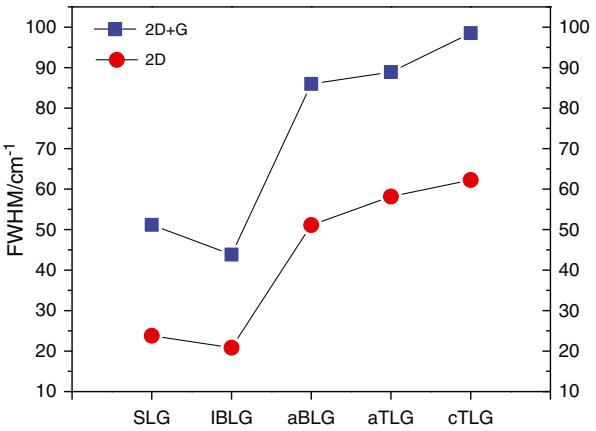

Figure 3. The FWHM of 2D and 2D + G bands vary as functions of graphene thickness and stacking sequence.

In addition to the FWHM and position, the intensity of Raman active mode is also one important parameter that can give useful information. Figure 5 shows the dependence of normalized Raman intensity on the thickness and stacking geometry for each mode (G, 2D, 2D′ and 2D + G). For each mode, the relative intensity of each graphene sample is normalized by its SLG intensity. The intensity of G band is strongly dependent on both thickness and stacking geometry, and it almost linearly increases with the thickness from SLG to aBLG and aTLG. Compared with the intensity of SLG's 2D band, the intensity does not show any increasing or decreasing tendency for Bernal/Rhombohedral stacking FLG despite the fact that the layer number is increased multiple times. For Bernal/Rhombohedral stacking FLG, the intensity of both 2D′ and 2D + G band show the same thickness dependent trend as that of the 2D band. It is worth noting that the IBLG present obvious stronger intensity compared with that of SLG for all Raman modes, which we discussed in this paper. This is because that in IBLG, the electronic coupling between

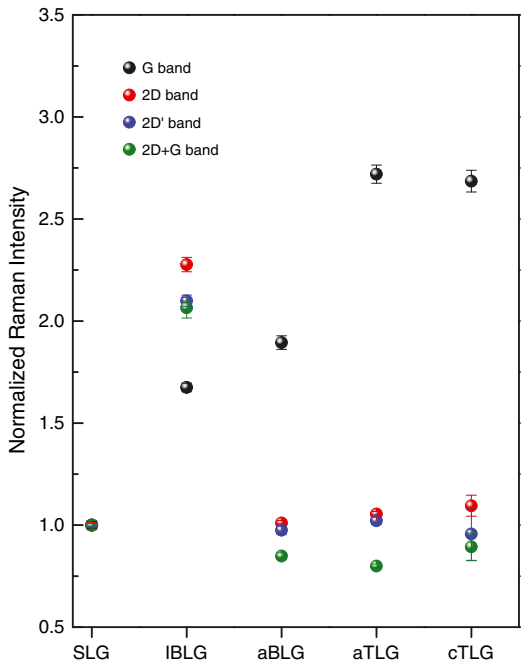

Figure 5. Raman intensity of G, 2D, 2D′ and 2D + G modes of SLG, IBLG, aBLG, aTLG and cTLG. The intensity of each mode is normalized by its SLG intensity. This figure is available in colour online at wileyonlinelibrary.com/journal/jrs

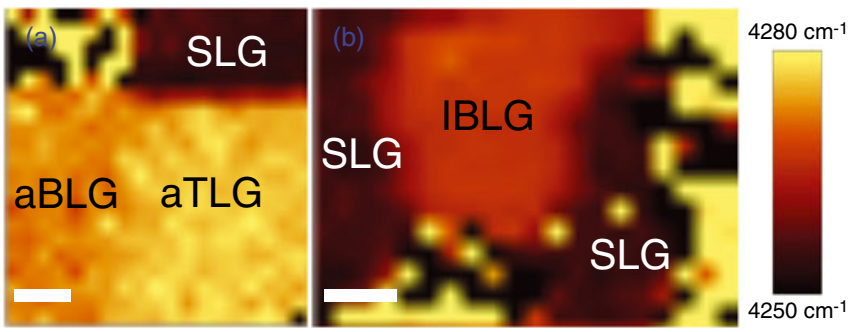

Figure 4. (a) Raman images of the band position of combination mode 2D + G (4200–4330 cm^{-1}) for SLG, aBLG, IBLG and aTLG. The scale bar is 0.7 μm for each image.

the two graphene layers are strongly suppressed, and hence the IBLG can be considered as two individual SLGs, which present two times intensity for each mode compared with that of SLG. To our best knowledge, the reason for the abnormal phenomenon that the intensity of 2D, 2D′ and 2D + G bands is independent of the thickness is still unclear to date. However, it is noticed that these three bands are all arising from multiphonon involved resonant Raman scattering processes. Theoretically, the multiphonon involved resonant Raman intensity is inversely proportional to the γ^2,[19,23] where γ is the scattering rate. Therefore, the scattering rate related to electron phonon interaction seems to be independent of the number of graphene layers for Bernal/Rhombohedral stacking. While for IBLG, the two-layer graphene cannot be considered as one system because of the lack of interlayer coupling; therefore, both the overtone and combination Raman intensity show twice of the intensity compared with that of SLG.

Conclusions

In summary, we have shown the evolution of high-order overtone and combination phonons 2D′ and 2D + G of graphene with thickness and stacking geometry. It is discovered that the Raman features of 2D + G band shows similar thickness and stacking geometry dependent trend as that of the 2D band, and the graphene's thickness and stacking geometry can be identified effectively by reading the peak position of 2D + G band. The case is totally different for 2D′ band because it always shows a single Lorentzian peak with fixed FWHM regardless of the thickness and stacking geometry. Furthermore, the intensity of each multiphonon involved resonant Raman mode in graphene is insensitive to the thickness for Bernal/Rhombohedral stacking FLG. The investigations of the Raman features of the high frequency Raman modes in graphene are of great importance because the 2D′ and 2D + G bands are resonant-scattering-based, which is directly related to the electronic and phonon band structures.

Acknowledgements

The work at SEU was supported by NSFC grant no.11144001 and 11104026, and at Jilin University was supported by Graduate Innovation Fund of Jilin University (Grant No. 20101055) and NSFC grant no.10974067.

Supporting information

Supporting information can be found in the online version of this article.

References

[1] Y. B. Zhang, Y. W. Tan, H. L. Stormer, P. Kim, *Nature* **2005**, *438*, 201.
[2] K. S. Novoselov, A. K. Geim, S. V. Morozov, D. Jiang, Y. Zhang, S. V. Dubonos, I. V. Grigorieva, A. A. Firsov *Science*, **2004**, *306*, 666.
[3] X. Zhu, H. B. Su, *J. Phys. Chem. C* **2010**, *114*, 17257.
[4] M. Y. Han, B. Ozyilmaz, Y. B. Zhang, P. Kim, *Phys. Rev. Lett.* **2007**, *98*, 206805.
[5] Y. B. Zhang, T. T. Tang, C. Girit, Z. Hao, M. C. Martin, A. Zettl, M. F. Crommie, Y. R. Shen, F. Wang, *Nature* **2009**, *459*, 820.
[6] S. Stankovich, D. A. Dikin, G. H. B. Dommett, K. M. Kohlhaas, E. J. Zimney, E. A. Stach, R. D. Piner, S. T. Nguyen, R. S. Ruoff, *Nature* **2006**, *442*, 282.
[7] Y. Hernandez, V. Nicolosi, M. Lotya, F. M. Blighe, Z. Y. Sun, S. De, I. T. McGovern, B. Holland, M. Byrne, Y. K. Gun'ko, J. J. Boland, P. Niraj, G. Duesberg, S. Krishnamurthy, R. Goodhue, J. Hutchison, V. Scardaci, A. C. Ferrari, J. N. Coleman, *Nat. Nanotechnol.* **2008**, *3*, 563.
[8] C. Berger, Z. M. Song, T. B. Li, X. B. Li, A. Y. Ogbazghi, R. Feng, Z. T. Dai, A. N. Marchenkov, E. H. Conrad, P. N. First, W. A. de Heer, *J. Phys. Chem. B* **2004**, *108*, 19912.
[9] S. Amini, J. Garay, G. X. Liu, A. A. Balandin, R. Abbaschian, *J. Appl. Phys.* **2010**, *108*, 094321.
[10] S. Amini, H. Kalaantari, J. Garay, A. A. Balandin, R. Abbaschian, *J. Mater. Sci.* **2011**, *46*, 6255.
[11] F. Parvizi, D. Teweldebrhan, S. Ghosh, I. Calizo, A. A. Balandin, H. Zhu, R. Abbaschian, *Micro & Nano Letters* **2008**, *3*, 29.
[12] K. S. Kim, Y. Zhao, H. Jang, S. Y. Lee, J. M. Kim, J. H. Ahn, P. Kim, J. Y. Choi, B. H. Hong, *Nature* **2009**, *457*, 706.
[13] X. S. Li, W. W. Cai, J. H. An, S. Kim, J. Nah, D. X. Yang, R. Piner, A. Velamakanni, I. Jung, E. Tutuc, S. K. Banerjee, L. Colombo, R. S. Ruoff, *Science* **2009**, *324*, 1312.
[14] A. C. Ferrari, *Solid State Commun.* **2007**, *143*, 47.
[15] L. M. Malard, M. A. Pimenta, G. Dresselhaus, M. S. Dresselhaus, *Phys. Rep.* **2009**, *473*, 51.
[16] M. A. Pimenta, G. Dresselhaus, M. S. Dresselhaus, L. G. Cancado, A. Jorio, R. Saito, *Phys. Chem. Chem. Phys.* **2007**, *9*, 1276.
[17] A. C. Ferrari, J. C. Meyer, V. Scardaci, C. Casiraghi, M. Lazzeri, F. Mauri, S. Piscanec, D. Jiang, K. S. Novoselov, S. Roth, A. K. Geim, *Phys. Rev. Lett.* **2006**, *97*, 187401.
[18] A. Das, S. Pisana, B. Chakraborty, S. Piscanec, S. K. Saha, U. V. Waghmare, K. S. Novoselov, H. R. Krishnamurthy, A. K. Geim, A. C. Ferrari, A. K. Sood, *Nat. Nanotechnol.* **2008**, *3*, 210.
[19] D. M. Basko, S. Piscanec, A. C. Ferrari, *Phys. Rev. B* **2009**, *80*, 165413.
[20] D. Zhan, L. Sun, Z. H. Ni, L. Liu, X. F. Fan, Y. Y. Wang, T. Yu, Y. M. Lam, W. Huang, Z. X. Shen, *Adv. Funct. Mater.* **2010**, *20*, 3504.
[21] W. J. Zhao, P. H. Tan, J. Liu, A. C. Ferrari, *J. Am. Chem. Soc.* **2011**, *133*, 5941.
[22] M. M. Lucchese, F. Stavale, E. H. M. Ferreira, C. Vilani, M. V. O. Moutinho, R. B. Capaz, C. A. Achete, A. Jorio, *Carbon* **2010**, *48*, 1592.
[23] S. Mathew, T. K. Chan, D. Zhan, K. Gopinadhan, A. R. Barman, M. B. H. Breese, S. Dhar, Z. X. Shen, T. Venkatesan, J. T. L. Thong, *Carbon* **2011**, *49*, 1720.
[24] D. Zhan, Z. H. Ni, W. Chen, L. Sun, Z. Q. Luo, L. F. Lai, T. Yu, A. T. S. Wee, Z. X. Shen, *Carbon* **2011**, *49*, 1362.
[25] Z. H. Ni, Y. Y. Wang, T. Yu, Y. M. You, Z. X. Shen, *Phys. Rev. B* **2008**, *77*, 235403.
[26] Z. H. Ni, L. Liu, Y. Y. Wang, Z. Zheng, L. J. Li, T. Yu, Z. X. Shen, *Phys. Rev. B* **2009**, *80*, 125404.
[27] A. A. Balandin, S. Ghosh, W. Z. Bao, I. Calizo, D. Teweldebrhan, F. Miao, C. N. Lau, *Nano Lett.* **2008**, *8*, 902.
[28] S. Ghosh, W. Z. Bao, D. L. Nika, S. Subrina, E. P. Pokatilov, C. N. Lau, A. A. Balandin, *Nat. Mater.* **2010**, *9*, 555.
[29] A. A. Balandin, *Nat. Mater.* **2011**, *10*, 569.
[30] Z. H. Ni, T. Yu, Y. H. Lu, Y. Y. Wang, Y. P. Feng, Z. X. Shen, *ACS Nano* **2008**, *2*, 2301.
[31] D. Yoon, Y. W. Son, H. Cheong, *Phys. Rev. Lett.* **2011**, *106*, 155502.
[32] Y. N. Xu, D. Zhan, L. Liu, H. Suo, Z. H. Ni, T. T. Nguyen, C. Zhao, Z. X. Shen, *ACS Nano* **2010**, *5*, 147.
[33] D. Zhan, L. Liu, Y. N. Xu, Z. H. Ni, J. X. Yan, C. Zhao, Z. X. Shen, *Sci. Rep.* **2011**, *1*, 12.
[34] Y. M. You, Z. H. Ni, T. Yu, Z. X. Shen, *Appl. Phys. Lett.* **2008**, *93*, 163112.
[35] S. S. Chen, Q. Z. Wu, C. Mishra, J. Y. Kang, H. J. Zhang, K. J. Cho, W. W. Cai, A. A. Balandin, R. S. Ruoff, *Nat. Mater.* **2012**, *11*, 203.
[36] R. Rao, R. Podila, R. Tsuchikawa, J. Katoch, D. Tishler, A. M. Rao, M. Ishigami, *ACS Nano* **2011**, *5*, 1594.
[37] C. X. Cong, T. Yu, R. Saito, G. F. Dresselhaus, M. S. Dresselhaus, *ACS Nano* **2011**, *5*, 1600.
[38] P. H. Tan, W. P. Han, W. J. Zhao, Z. H. Wu, K. Chang, H. Wang, Y. F. Wang, N. Bonini, N. Marzari, N. Pugno, G. Savini, A. Lombardo, A. C. Ferrari, *Nat. Mater.* **2012**, *11*, 294.
[39] Y. Kawashima, G. Katagiri, *Phys. Rev. B* **1995**, *52*, 10053.
[40] Z. H. Ni, H. M. Wang, J. Kasim, H. M. Fan, T. Yu, Y. H. Wu, Y. P. Feng, Z. X. Shen, *Nano Lett.* **2007**, *7*, 2758.
[41] I. Calizo, I. Bejenari, M. Rahman, G. Liu, A. A. Balandin, *J. Appl. Phys.* **2009**, *106*, 043509.
[42] P. Giannozzi, S. Baroni, N. Bonini, M. Calandra, R. Car, C. Cavazzoni, D. Ceresoli, G. L. Chiarotti, M. Cococcioni, I. Dabo, A. Dal Corso, S. de Gironcoli, S. Fabris, G. Fratesi, R. Gebauer, U. Gerstmann, C. Gougoussis, A. Kokalj, M. Lazzeri, L. Martin-Samos, N. Marzari, F. Mauri, R. Mazzarello, S. Paolini, A. Pasquarello, L. Paulatto, C. Sbraccia,

S. Scandolo, G. Sclauzero, A. P. Seitsonen, A. Smogunov, P. Umari, R. M. Wentzcovitch, *J. Phys. Condens. Matter* **2009**, *21*, 395502.
[43] N. Troullier, J. L. Martins, *Phys. Rev. B* **1991**, *43*, 1993.
[44] M. Methfessel, A. T. Paxton, *Phys. Rev. B* **1989**, *40*, 3616.
[45] S. Baroni, S. de Gironcoli, A. Dal Corso, P. Giannozzi, *Rev. Mod. Phys.* **2001**, *73*, 515.
[46] C. X. Cong, T. Yu, K. Sato, J. Z. Shang, R. Saito, G. F. Dresselhaus, M. S. Dresselhaus, *ACS Nano* **2011**, *5*, 8760.
[47] C. H. Lui, Z. Q. Li, Z. Y. Chen, P. V. Klimov, L. E. Brus, T. F. Heinz, *Nano Lett.* **2011**, *11*, 164.
[48] C. Thomsen, S. Reich, *Phys. Rev. Lett.* **2000**, *85*, 5214.
[49] S. B. Trickey, F. Mullerplathe, G. H. F. Diercksen, J. C. Boettger, *Phys. Rev. B* **1992**, *45*, 4460.
[50] S. Y. Zhou, G. H. Gweon, J. Graf, A. V. Fedorov, C. D. Spataru, R. D. Diehl, Y. Kopelevich, D. H. Lee, S. G. Louie, A. Lanzara, *Nat. Phys.* **2006**, *2*, 595.
[51] J. A. Yan, W. Y. Ruan, M. Y. Chou, *Phys. Rev. B* **2008**, *77*, 125401.